Wasit Journal of Engineering Sciences

Journal homepage: https://ejuow.uowasit.edu.iq

Numerical Study of Improving Solar Chimney Performance by using Energy Storage

Tuqa Abduljabbar [1], Abbas J. Jubear[1], Batool M.Faisal[1]

Affiliations
[1]Department of Mechanical Engineering,
Wasit University,
Wasit, Iraq.

Correspondence
Tuqa Abdul Jabbar,
tukaj301@uowasit.edu.iq

Received
21-September-2022
Revised
24-October-2022
Accepted
2-November-2022

Doi: 10.31185/ejuow.Vol10.Iss3.374

Abstract

In this study, a simulation for two story building associated with a vertical solar chimney was made by using ANSYS 2022/R1. The study conducted under the climatic conditions of Al-kut city/ Iraq on 5/8/2016. The study involved a comparison between the ventilation performance of SC before and after adding Energy Storage. Al-dura, RT-42, and block-shaped paraffin wax were the three types of PCM that were studied in order to find the optimum ES. The numerical results showed that the best Paraffin wax was Al-dura depending on the average Air Change per Hour (ACH), average indoor temperature, and the ventilation period after sunset. Comparing with the 1st model (without ES), After adding Al-dura wax, the ACH increased by 18.3 % and 9.95 % for 1st and 2nd floor, respectively. whereas, the indoor temperature was reduced by 1.17 k and 0.68 k on the 1st and 2nd floor, respectively. As for the ventilation period, it was lasted for 5 h after sunset.

Keywords: ACH, ANSYS, energy storage, natural ventilation, PCM, solar chimney

الخلاصة: في هذه الدراسة، تم إجراء محاكاة لمبنى مكون من طابقين مرتبط بمدخنة شمسية عمودية باستخدام ANSYS 2022 / R1. أجريت الدراسة في ظل الظروف المناخية لمدينة الكوت / العراق بتاريخ ٢٠١٦/٨/٥. اشتملت الدراسة على مقارنة أداء تهوية المدخنة الشمسية قبل وبعد إضافة مادة خزن الطاقة. تم المقارنة بين اداء ثلاث انواع من المواد متغيرة الطور وهي شمع الدورة وRT42 و شمع برافين على شكل كتلة من أجل إيجاد النوع الأمثل. أوضحت النتائج العددية أن أفضل شمع برافين هو شمع الدورة بالاعتماد على متوسط عدد مرات تغير الهواء بالساعة ACH ومعدل درجة الحرارة الداخلية وفترة التهوية بعد غروب الشمس. بينت النتائج انه بالمقارنة مع النموذج الاول (الذي لا يحتوي مادة خزن طاقة)، فان إضافة شمع الدورة زاد من معدل ACH بنسبة ١٨,٣٪ و ٩,٩٥٪ للطابقين الأول والثاني على التوالي. بينما انخفضت درجة الحرارة الداخلية بمقدار ١,١٧ كلفن و ٠,٦٧٥ كلفن في الطابق الأول والثاني على التوالي. وزادت فترة التهوية بمقدار ٥ ساعات بعد غروب الشمس.

1. INTRODUCTION

In very hot summer climates, ventilation and air conditioning are essential, but for environmental reasons and lack of Electrical energy, it is better to find alternatives such as natural ventilation by solar chimney. In general, ventilation is the process of exchanging air between indoor and outdoor environments to loosen and remove indoor air containment. Moreover, ventilation is a useful solution for achieving thermal comfort conditions and is divided into two types: mechanical (forced) and natural ventilation. Mechanical ventilation requires the generated electrical energy (EE), while natural ventilation depends on wind and thermal buoyancy as the driving force. The thermal buoyancy effect can be produced by using the solar chimney, which is an air channel containing holes for air to

enter and depart. The air in this channel is heated by solar radiation, causing hot air to rise as a result of a reduction in its density and to exit from the chimney's top exit hole, which causes air to withdraw from the air intake holes. Building ventilation and power generation utilize this technology. However, the solar chimney works during sunlight times and stops working after sunset, so adding Energy Storage ES is necessary to elongate the period of ventilation. ES is used in SCs to store part of solar thermal energy during sunlight times to make use of it after sunset. ES can be classified in to three categories: electrical, mechanical, and thermal. In SCs application, the thermal ES is used which is also classified in to Sensible heat energy storage SHS and Latent heat energy storage LHS. LHS is mainly appealing own to its capacity to provide a high ES density and for heat storing at a constant temperature equivalent to the phase transition temperature of phase change materials (PCM). It is possible to switch between solid phase, liquid solid, solid gas, liquid gas, and vice versa. Numerous scientific studies have been done in this area in an effort to enhance the performance of the solar chimney and discover the best design that meets the comfort requirements inside the buildings, including those that addressed the design of the chimney in terms of dimensions and angles of inclination and those including what added additional parts like energy storage or passive cooling systems. Saleem et al. [1] numerically studied several dimensions of SC under real climatic operation conditions of Alexandria, Egypt in summer for the days (1st to 7th of August). Findings revealed the best design of the SC was 1.4 m, 0.6 m, and 0.10 m in length, width, and air gap, respectively along with 45° inclination angle. Shi et al. [2] studied the effects of various factors on the performance of SCs in buildings. According to the findings, the best SC design includes a height/gap ratio of around 10, equal outlet and inlet, a gap of cavity (0.2–0.3) m, an angle of inclination 45–60° (for roof SC including latitude), double/triple glazing, a suitable opening of the room, an insulation wall of 5 cm in thickness, and a higher emissivity and absorptivity solar absorber. Jubear and Ghareer [3] simulated several models of the SCs by ANSYS fluent, for enhancing the natural room ventilation in (Al-Kut/Iraq) during the hot summer climate. The study showed that the optimum thermal performance was verified by these conditions: [45^{o} inclination angle, the south orientation in case of one SC, and in case of two SCs (one on the south and the other on the west)]. Hashim et al. [4] conducted a numerical analysis to improve natural ventilation in different SC models inside a room based on the notions of the traditional chimney model. When compared to a traditional chimney model, they found that, the vertical extended and inclined chimneys enhanced rate of ventilation by 13% and 7.5 %, respectively. Mohammed et. al. (2020) [5] statistically explored the natural ventilation in two-story buildings using a vertical two-story SC passive system by using ANSYS fluent. The results showed that the long vertical SC might provide the optimum NV while also causing a visible rise in inside temperatures. Herouane et al. [6] made a numerical simulation by ANSYS fluent for a rooftop solar chimney associated with a 3 m height square room. Three side lengths were involved 3, 4, and 5 m. Results showed that the optimum air velocity, air flow, and kinetic energy were 2.88 m/s, 180 m^3/hrs., and 5.15 m^2/s^2, respectively. These values was achieved when the side length was 4 m. Kaneko et al. [7] investigated the possibility of elongation of natural ventilation during evening and night time by using PCM within the SC. The simulated results showed a stable flow rate all day while the measured flow rate was changing every time at night. The prototype SC provides an airflow rate of 100 to 400 m^3/h. Safari and Torabi (2014) [8] conducted a numerical study to improve the thermal performance of a PCM-based SC integrated into a guardroom for a passive solar heating system. Findings indicated that the utilization of PCM in SC kept the temperature levels almost uniform in the guard room for the whole day, while without PCM the temperature varies both day and night time. Bin et. al. [9] studied experimentally the influence of the location of PCM ($Na_2CO_3.10H_2O$) on the SC in a hybrid wall. It was concluded that for effective energy storage PCM should not expose to direct radiation. Salari et al. [10] conducted a numerical study on the inclined rooftop SC performance with phase change material and a photovoltaic module called (SC-PV-PCM) system. It was concluded that for residential buildings the best choice was the SC-PV-PCM system, on the other hand, for office building SC-PV was the best option. Long et. al. [11] investigated the effects of integrating the solar chimney with PCM and EAHE, numerically. They found that the temperature of chamber associated with the SC was varied from (25.1-28.4) °C in case of with PCM and the temperature varied from (25.1-29.2) °C in case of no PCM. As for the current study, its conducted under the climatic conditions of Al-kut city, that is located in the middle east of Iraq at longitude (E°45.78) and latitude (N°32.54). The city's climate is considered extreme, as it is cold and humid in winter and hot and dry in summer.

2. AIM OF THE STUDY

The main aim of this work is to enhance the efficiency of a solar chimney by adding phase change material as ES to elongate the natural ventilation process after sundown in a two-story building.

3. CFD MODELLING ANALYSIS

The computational fluid dynamic consisted of several steps, beginning with the designing the geometry, generating the mesh, and determining the governing equations and the assumptions of the boundary conditions. In this section, two models were simulated. The 1st model was a simulation for the solar chimney and two-story building only. Whereas the 2nd model was adding the energy storage to the 1st model. The study consisted of a comparison of the ventilation performance by the solar chimney in the two models.

3.1 Geometrical design

The first model consisted of the two-story building that was made of wood. Each room was (1×1×1) m^3. The thickness of the walls was (8) mm. The building consisted of one inlet opening and one outlet opening for each room. The dimension of the inlet opening was (0.3×0.3) m^2 through which the air is exchanged between the outdoor and room inside, while the outlet opening dimension was (1×0.3) m^2 through which the air is exchanged between the room and SC. The building was connected with a vertical SC from the south direction. The SC is (3) m long, (1) m width, and (0.3) m air gap. The glass facade is (4) mm in thickness. The absorber wall that collects and reflects the solar radiation is of (1) mm thickness of Aluminum plate. The thickness of the glass wool that thermally isolated the building from the chimney was (50) mm. The roof of the building is insulated by (25) mm insulation layer. The thermal properties of the materials are illustrated in the table 1, while Figure 1 shows the building and SC.

Table 1 The thermal properties of the materials [12]

Material	Thickness mm	Density (ρ) Kg/m^3	Specific heat KJ/kg.k	Thermal conductivity W/m.k	Absorptivity (α)	Emmisivity (ε)	Transmisivity (T)
Glass	4	2220	0.83	1.15	0.06	0.95	0.84
Aluminum	1	2700	0.9	273	0.95	0.95	0
Wood	8	400	1.8	0.06	0.5	0.5	0
Insulator	50&25	52	0.657	0.038	0.4	0.4	0

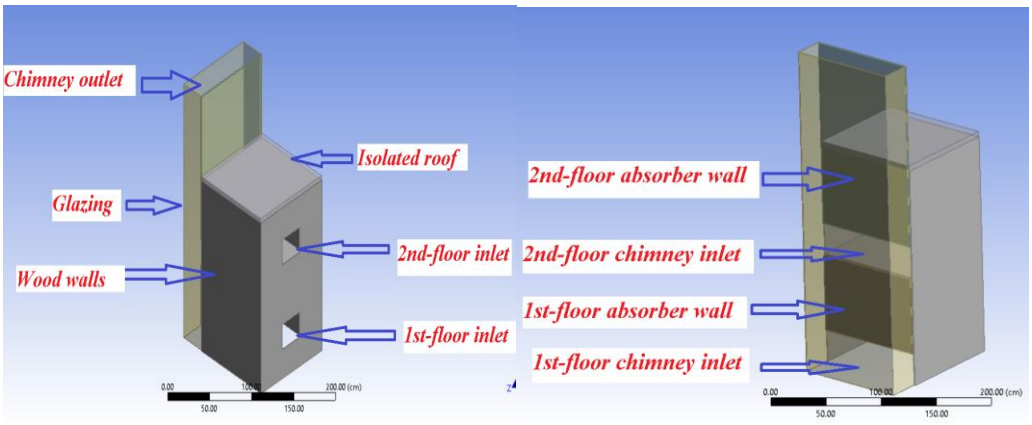

Figure 1 The two-story building and solar chimney

Regarding the 2nd model, three types of wax were used as ES in the SC namely: Al-dura , RT-42, and block-shaped paraffin wax. The thermo-physical properties of the three types of wax are illustrated in the table 2. The wax was placed between the absorber wall and the insolation layer on the first floor. The dimensions of the wax container were (0.7 m in length × 1 m in width). The specific heat was assumed to be 2000 J/kg.k, while the heat of fusion

was assumed equal to 250 KJ/kg for all wax types as per the previous studies (except for RT-42 when the specific heat and heat of fusion are 2400 J/kg. k and 174000 J/kg, respectively). The thickness of wax layer was (4) cm.

Table 2 The thermo-physical properties of the wax

Phase change material	Density (kg/m^3)	Thermal conductivity (W/m.k)	Viscosity (kg/m.s)	Liquidus temperature (K)
Al-Dura paraffin wax	785.2	0.3285	0.01	325.5
Block-shaped paraffin wax	800.516	0.257	0.016	329.5
RT-42 paraffin wax [13]	760	0.2	0.01	316

3.2 Mesh generation

The optimum mesh was chosen depending on the mesh independence study conducted on the 1st model (two story building with the SC), where the value tested was the ACH on the 1st and 2nd floor at 12 p.m. Figure 2 shows that the optimum number of cells was in the range of (1500000,1900000, and 2500000), when the ACH were (9.2, 9.5, and 9.7, respectively) for the 1st floor, whereas ACH were (8.5, 9, and 9.2, respectively) for the 2nd floor. The value chosen was (1900000) because the difference in results was minor, in addition to the fact that using a small number of cells would speed up the solution. The values of mesh metrics and the number of cells is illustrated in the table 3. Figure 3 shows the type of mesh used in simulation was hexagonal mesh.

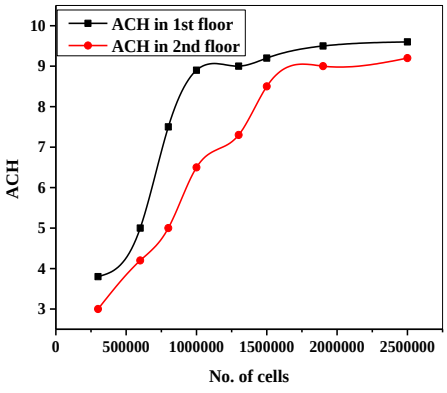

Figure 2 Mesh independence study

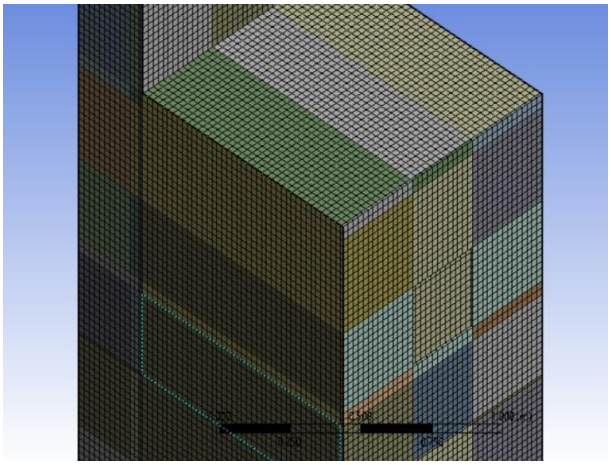

Figure 3 Mesh of two-story building and SC

Table 3 Optimum mesh properties

Max. Aspect ratio	Max. Skewness	Orthogonality	No. of Cells
5.0882	1.3177e-010	0.985	1900000

3.3 Governing equations

The flow of air in the solar chimney is caused by natural convection due to solar radiation. The governing equations used in the simulation consist of the Reynolds Averaged Navier – Stokes (RANS) equations along with continuity, energy, turbulence, and radiation transfer equation [14] and [15]. These are as follows:

3.3.1 Conservation of Mass (the continuity equation)

For transient and three dimensions of the incompressible flow, The equation for conservation of mass, or continuity equation, can be written as follows[14]:

$$\frac{\partial \rho}{\partial t} + \nabla \cdot (\rho \vec{v}) = 0 \quad (1)$$

3.3.2 Momentum Equations (Conservation of Momentum)

In physics, the Navier–Stokes equations are certain partial differential equations that describe the motion of viscous fluid substances, The Navier–Stokes equations mathematically express the conservation of momentum and conservation of mass for Newtonian fluids. Conservation of momentum in an inertial (non-accelerating) reference frame is described by[15]:

$$\frac{\partial}{\partial t}(\rho \vec{v}) + \nabla \cdot (\rho \vec{v} \vec{v}) = -\nabla p + \nabla \cdot (\bar{\bar{\tau}}) + \rho \vec{g} \quad (2)$$

Where p is the static pressure, $\bar{\bar{\tau}}$ is the stress tensor described below:-

$$\bar{\bar{\tau}} = \mu \left[(\nabla \vec{v} + \nabla \vec{v}^{\mathrm{T}}) - \frac{2}{3} \nabla \cdot \vec{v} I \right] \quad (3)$$

Where μ is the molecular viscosity, I is the unit tensor, and the second term on the right hand side is the effect of volume dilation.

While ρg is the Boussinesq assumption that used for the change in the density of Air as follows:

$$\rho g \approx \rho_0 \big(1 - \beta (T - T_o)\big) g \quad (4)$$

Where:

ρ_0: The reference density of air (kg/m^3)

β: The thermal expansion coefficient of air (1/K)

T_o: The ambient temperature (K)

3.3.3 Energy Equation

ANSYS FLUENT solves the energy equation in the following form [15]:

$$\frac{\partial}{\partial t}(\rho E) + \nabla \cdot \left(\vec{v}(\rho E + p) \right) = \nabla \cdot \left(k_{\text{eff}} \nabla T - \sum_j h_j \vec{J}_j + (\bar{\bar{\tau}}_{\text{eff}} \cdot \vec{v}) \right) + S_h \quad (5)$$

Where k_{eff} is the effective conductivity (k+kt, where kt is the turbulent thermal conductivity, defined according to the turbulence model being used), and $\vec{J}_j$ is the diffusion flux of species j. the first three terms on the right-hand side of Equation (5) represent energy transfer due to conduction, species diffusion, and viscous dissipation, respectively. S_h includes the heat of chemical reaction, and any other volumetric heat sources.

3.3.4 K-epsilon Turbulence equations

The K-Epsilon model was used to simulate turbulent air flow. This model uses the equations below to represent the airflow process[15].

$$\rho \nabla \cdot \left(\vec{v} k \right) = \nabla \cdot \left[\left(\mu + \frac{\mu_t}{\delta_k} \right) \nabla k \right] + G_k + G_b - \rho \varepsilon \quad (6)$$

$$\rho \nabla \cdot \left(\vec{v} \varepsilon \right) = \frac{\partial}{\partial x_j} \left[\left(\mu + \frac{\mu_t}{\delta_\varepsilon} \right) \frac{\partial \varepsilon}{\partial x_j} \right] + C_{1\varepsilon} \frac{\varepsilon}{k} (G_k + C_{3\varepsilon} G_b) - C_{2\varepsilon} \rho \frac{\varepsilon^2}{k} \quad (7)$$

3.3.5 Modeling Radiation

The following equation [15] illustrates how the radiation transfer equation (RTE) is used to describe the solar radiation behavior according to absorb, dissipate, and emit, the director r towards the director s.

$$\rho \nabla \cdot \left(\vec{v} \varepsilon \right) = \frac{\partial}{\partial x_j} \left[\left(\mu + \frac{\mu_t}{\delta_\varepsilon} \right) \frac{\partial \varepsilon}{\partial x_j} \right] + C_{1\varepsilon} \frac{\varepsilon}{k} (G_k + C_{3\varepsilon} G_b) - C_{2\varepsilon} \rho \frac{\varepsilon^2}{k} \quad (8)$$

3.4 Assumptions of The Boundary Conditions

The assumption used in the software were as follows:

- Transient-state conditions.

- Turbulent flow.
- Three dimensional.
- The Boussinesq approximation is utilized.
- Incompressible flow.
- The specific heats are the same for all the wax types equal 2000 J/kg.k. depending on various researches (except for RT42).
- The heat of fusion is the same for all the wax types which equals 250000 J/kg depending on various researches (except for RT42).
- Constant properties of PCMs.

The present work occurred under the climatic conditions of Al-Kut city on (5-8-2016) with a constant intervals hours (6:00 am to 6:00 am in the following day). Table 4 depicts the climatic conditions of this day according to the Iraqi Agro meteorological network.

Table 4 Climatic Data of Al-Kut City on (5/8/2016)

Hour	Solar intensity (W/m^2)	Ambient temperature (K)	Average wind speed (m/s)	Relative humidity %
6:00 am	11.18	305.5		19
8:00 am	288.47	311.5		21
10:00 am	687.08	316.5		10
12:00 pm	802.76	320.5		9
2:00 pm	741.51	320.6		8
4:00 pm	443.86	318.6	0.66	8
6:00 pm	124.45	313	.	12
8:00 pm	0	308.5	.	14
10:00 pm	0	304	.	14
12:00 am	0	302	2.55	24
2:00 am	0	302.5		24
4:00 am	0	303		20
6:00 am	12	305		19.5

3.5 Assumptions of The Boundary Conditions

The boundary conditions are characterization to the thermal variables on the border of the typical CFD simulation model. Therefore, the boundary condition has a significant effect on the numerical analysis results of the model while using Ansys Fluent software. The following are the boundary conditions details for each component where the inlet and outlet temperatures have been written as polynomial equations representing the actual 24-hours data, then hooked up to Fluent software and recalled from the boundary condition tap, the heat transfer coefficient from the walls of the room to the ambient is also calculated and inserted into the Fluent as per the wind velocity at the experiment location for the whole 24-hour period and is shown below in equation (9) [16]:

$$h_{conv}=h_{wind}=5.7 \times 3.8\, V_{wind} \quad (9)$$

The 1st and 2nd models boundary conditions are illustrated in the table (5).

Table 5 Boundary conditions of 1st and 2nd model

Boundary	Type	Boundary condition	Value
Inlet	Entrance	Pressure, temperature inlet	P_{in}=0 pa, $T_{in}=T_{amb}$ k
Outlet	Outlet	Pressure, temperature outlet	P_{out}=0 pa, $T_{out}=T_{amb}$ k
Glass	Semitransparent wall	Mixed (convection and radiation)	$h=h_{wind}$, $T=T_{amb}$, $T_{sky}=0.0552* T_{amb}^{1.5}$,

			Solar radiation
Side walls	Opaque wall	Convection	$h=h_{wind}$, $T=T_{amb}$
Ceiling	Opaque wall	Convection	$h=h_{wind}$, $T=T_{amb}$
Ground	Opaque wall	Insulation	Heat flux =0 W/m^2

4 VALIDATION

The validation of the present work depends on the comparison with the experimental work for a single-floor room model with an inclined solar chimney, which is accomplished by Ahmed et. al [17]. The thermal specifications for all design materials and the ambient thermal conditions of temperatures and solar radiation were used. The present CFD simulation was carried out for six hours, with one hour between each reading, from 10 a.m. to 3 p.m.. The validation consisted of a comparison between the experiment results of published work and the present numerical work. Good agreement was accomplished between the results. Where the percentage of variation in the results was (2.02 %) in absorber temperature, while the percentage of variation in the results was (9.6 %) in air velocity at the chimney inlet. Figures (4) and (5) present the validations charts.

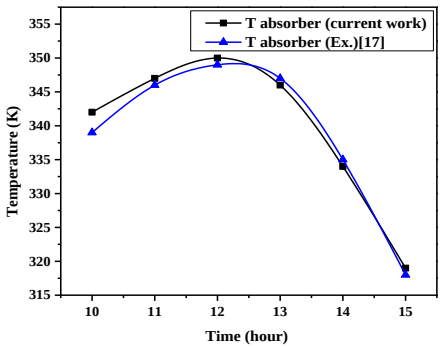

Figure 4 The absorber temperature comparison of Validation

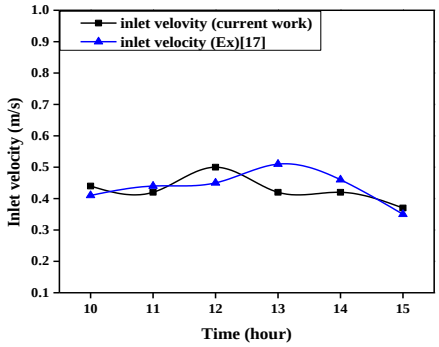

Figure 5 The chimney inlet velocity comparison of Validation

5 RESULTS AND DISCUSSIONS

5.1 Thermal performance of the first model (without ES)

As previously mentioned, this model consisted of a simulation for the two-story building and the solar chimney. The thermal performance of solar chimney ventilation was examined according to three factors: ACH, indoor average temperature, and the number of hours of ventilation.

Regarding ACH, Figure 6 shows that the maximum ACH values on the 1st floor and 2nd floor were 12 and 11, respectively registered at 12 p.m. when the solar radiation intensity was 802.76 W/m^2. Whereas, the minimum values that recorded through the daylight period were 4 and 3.5 at 8 a.m. on the 1st and 2nd floor that is registered when the solar radiation intensity was 288.47 W/m^2. In this model, it was found that average ACH were 4.833 and 4.85 for 1st and 2nd floors, respectively.

After sunset, the values stabilized on 2 on the 1st floor and 3 on 2nd floor and that is because of the absence of solar radiation which warming the absorber wall that in turn reflects the thermal radiation on the air in the air gap producing low density air flowing up and in sequence suctioning fresh air from the rooms inlets.

The Figure also shows that in the daylight, the ACH values on the 1st floor were higher than the ACH values on the 2nd floor and that is due to the first level's solar chimney column being one meter longer than the second floor's, the first floor has a greater buoyancy impact than the second floor. As a result, the first floor chimney coupling hatch has a higher air intake rate than the second story chimney coupling hatch. Whereas, during the night the ACH values on the 1st floor is less than the ACH values on the 2nd floor that is because the absence of buoyancy affect and the air flows in reverse path from SC to the rooms that led to velocity drop due to the friction losses that increased with the increasing of air path length.

As for the indoor temperatures, Figure 7 shows that the maximum indoor temperature were 323 K on the 1st floor and 323.5 K on the 2nd floor recorded at 2 p.m. and 4 p.m. when the solar radiation was in the range of (741.51-443.86) W/m^2 and the ambient temperature was 320.6 K. Whereas, the minimum indoor temperature was 303 K and 302 K on the 1st and 2nd floor, respectively at 4 a.m. and 6 a.m.. The average indoor temperature in the 1st and 2nd floors were 312.875 k and 312.625 k, respectively while the outdoor average temperature was 310.558 k. The reason behind the indoor temperature be in higher temperature than the ambient is due to a portion of the air being stagnant in the higher regions of the rooms and being heated by the walls' exposure to solar radiation during daytime hours.
The results of simulation shows the ACH and the indoor temperatures would being rising according to the solar intensities and ambient temperatures rising and vise-versa. Regarding the ventilation process that happened due to buoyancy effect was started at 8 a.m. and ended at 6 p.m. after that, the ventilation was in reverse flow and ACH stabilized at 2 and 3 on 1st and 2nd floors, respectively. Figures 8 to 11 show the velocity vectors and temperature contours at 12 p.m. and 12 a.m., respectively.

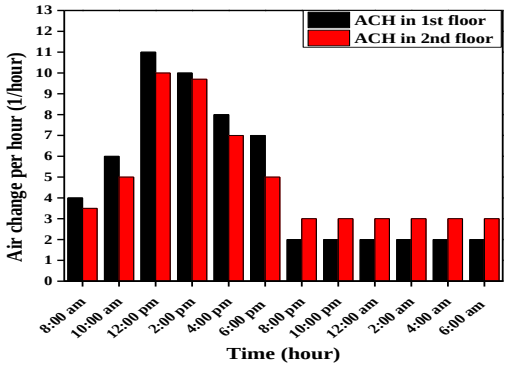

Figure 6 ACH values of 1st model

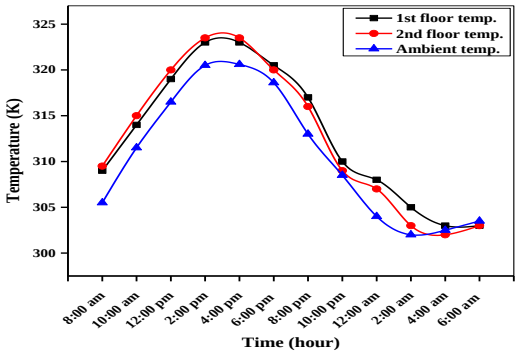

Figure 7 Average temperature values in 1st model

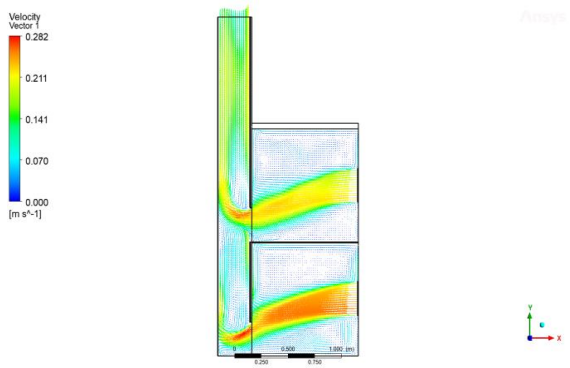

Figure 8 Velocity vector of 1st model at 12 p.m.

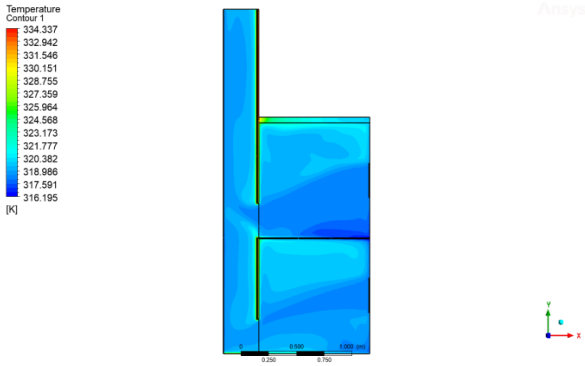

Figure 9 Temperature contour of 1st model at 12 p.m.

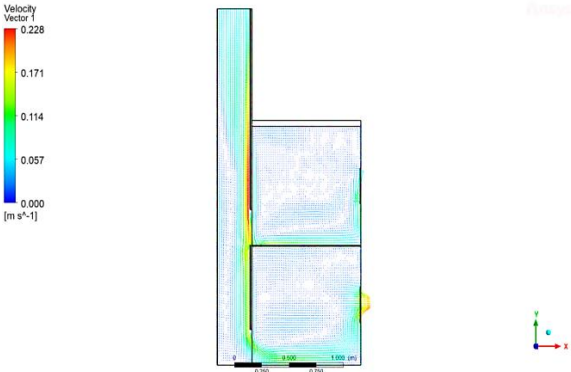

Figure 10 Velocity vector of 1st model at 12 a.m.

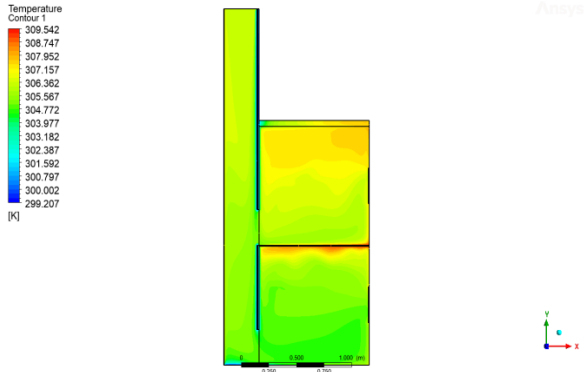

Figure 11 Temperature contour of 1st model at 12 a.m.

5.2 Thermal performance of the second model

This model consisted of a simulation for the two-story building, the SC and the ES that is located behind the absorber on the first floor. Its aimed to study the effect of changing the ES type on thermal performance of SC. Three types of paraffin wax with a thickness of 4 cm were used in the numerical study namely: Al-dura paraffin wax, Block-shaped paraffin wax, and RT-42 paraffin wax.

5.2.1 Al-dura paraffin wax

This case includes the building with the SC and Al-dura paraffin wax as ES. The thermal performance of solar chimney ventilation was examined according to three factors: ACH, indoor temperature, and The total number of hours of ventilation.

On the 1st floor, The maximum ACH was recorded at 4 p.m. which was equal to 10 while the minimum ACH was 2 from 2 a.m. to 6 a.m.. on the other hand, the maximum ACH on the 2nd floor was 9.5 at 2 p.m. while the minimum value was 3 at 2 a.m. to 6 a.m. The average ACH on 1st and 2nd floors were 5.716 and 5.333, respectively. Figure 12 illustrates the ACH values according to time.

Regarding the indoor temperature, the maximum value on the 1st floor recorded was 321 K at 2 p.m. and 4 p.m., while the minimum value was 303 K at 4 a.m. and 6 a.m. On the other hand, the maximum recorded temperature on the 2nd floor was 322 K at 2 p.m. and 4 p.m., while the minimum temperature was 302 K recorded at 4 a.m.. Figure 13 illustrates the temperature values according to test periods. It was found that the average indoor temperature for 1st and 2nd floors were 311.708 k and 311.95 k, respectively

The ventilation started at 8 a.m. and ended at 12 a.m. on the next day, depending on the values of the ACH, which changes during these hours and then stabilized at fixed values after 12 a.m.. To demonstrate the behavior of temperature and air velocity through the day and night periods when using this type of wax in this thickness, figures 14 to 17 illustrate the velocity vectors and temperature contours at 12 p.m. and 12 a.m..

The process of melting and solidification of wax had an impact on the ventilation because the temperature of the wax affects the temperature of the absorbent wall, which affects the temperature of the air adjacent to the absorber wall, and that in turn affects the velocity of air in SC. However, this does not mean that the ventilation process has completely stopped after the wax has solidified, that means the ACH will not be equal to zero, because ventilation occurs as a result of the pressure difference caused by the difference in air temperatures between the building and the outside environment. Figures 18 and 19 illustrate the liquid fraction at 12 p.m. and 12 a.m., respectively, where the simulation results showed that the average liquid fraction at these times were 0.4 at both times.

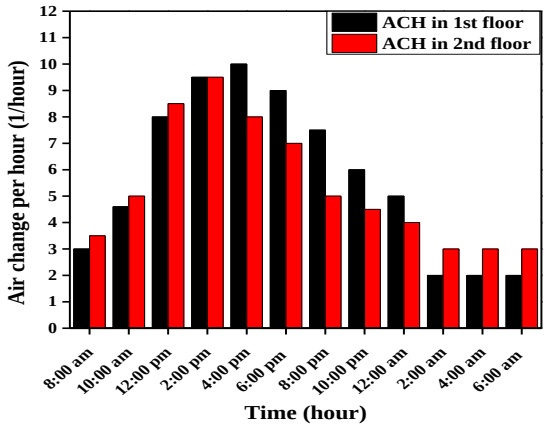

Figure 12 ACH values when using Al-dura Paraffin wax

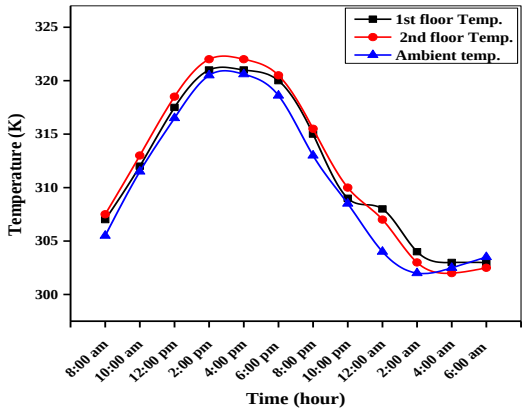

Figure 13 Average temperature when using Al-dura wax

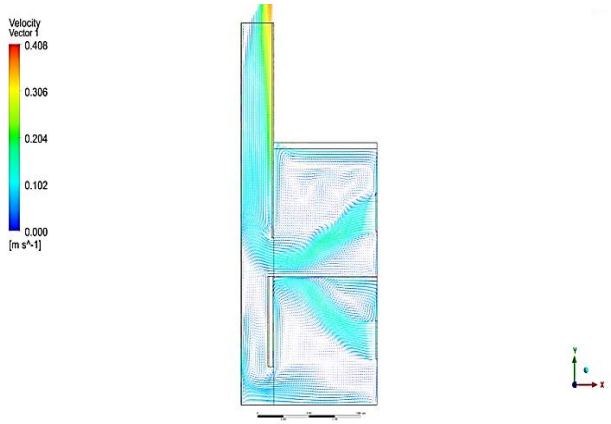

Figure 14 Velocity vector when using Al-dura wax at 12 p.m.

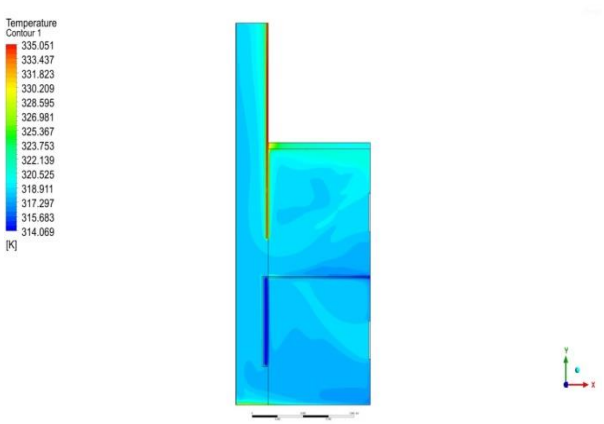

Figure 15 Temperature Contour when using Al-dura wax at 12 p.m.

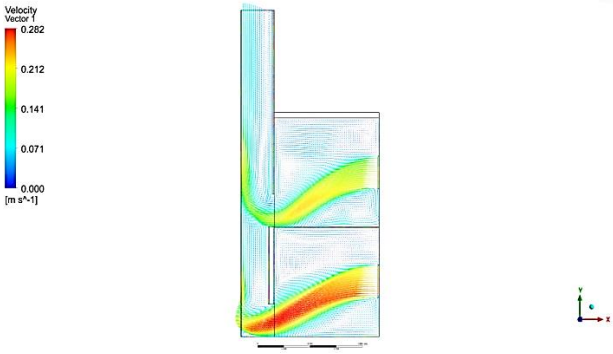

Figure 16 Velocity vector when using Al-dura wax at 12 a.m.

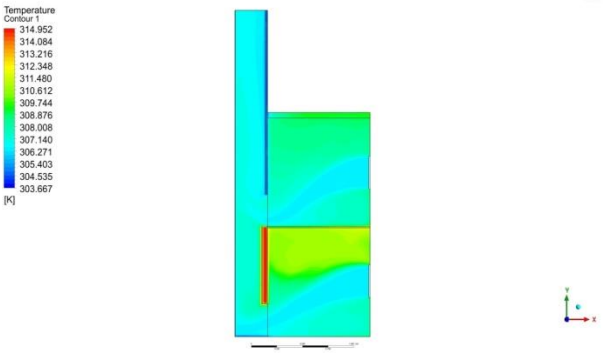

Figure 17 Temperature Contour when using Al-dura wax at 12 a.m.

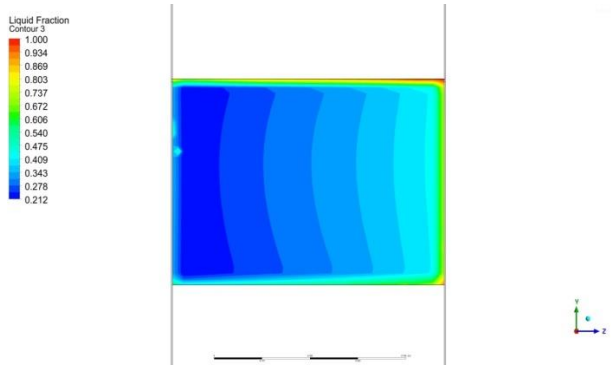

Figure 18 Liquid fraction contour of Al-dura wax at 12 p.m.

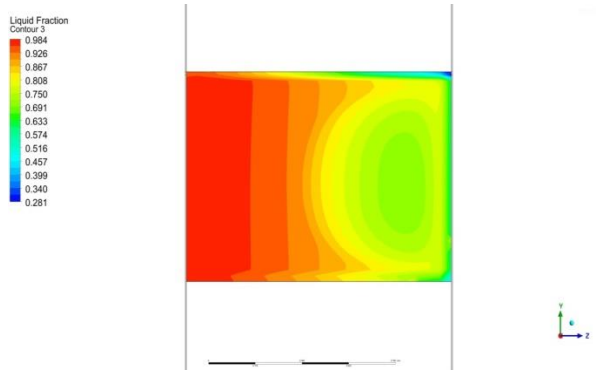

Figure 19 Liquid fraction contour of Al-dura wax at 12 a.m.

5.2.2. Block-shaped paraffin wax

In this case, Block-shaped paraffin wax was used as ES. As in the previous case, the results of the second numerical model are dealing with the ACH, the indoor temperatures of the two-story building during the simulation test periods, and the number of hours of ventilation.

The maximum ACH of the 1st floor was 9 which occurred at 2 p.m., while the minimum value was 2 registered at 10 p.m. till 6 a.m. On the other side, the highest and lowest levels of (ACH) on the second floor are 9.5 at 2 p.m. and 3 at 10 p.m. till 6 a.m. respectively, as seen in Figure 20. The average ACH on 1st and 2nd floors were 4.475 and 4.65, respectively.

In terms of indoor temperature, the maximum recorded temperature on the 1st floor was 322 k at 2 p.m. and 4 p.m., while the minimum temperature on the same floor was 303 k recorded at 4 a.m. and 6 a.m .. On the other hand, the maximum temperature on the 2nd floor was 323.5 k recorded at 4 p.m., while the minimum temperature recorded

was 302 k at 4 a.m .. Figure 21 showed the temperature distribution on the two story building. Results showed that average indoor temperature on the 1st and 2nd floors were 312.166 k and 312.208 k, respectively.
In this type of wax the ventilation process started at 8 a.m. and ended at 8 p.m.. Figures 22 to 27 illustrate the velocity vectors, temperature contours, and liquid fraction contours at 12 p.m. and 8 p.m.. The velocity vector in the figure 24 demonstrates that at 8:00 pm the ventilation due to buoyancy effect confined only on the 1st floor, while its stops at the 2nd floor and that is due to temperature difference between air temperature in first floor air exit and the top of chimney.

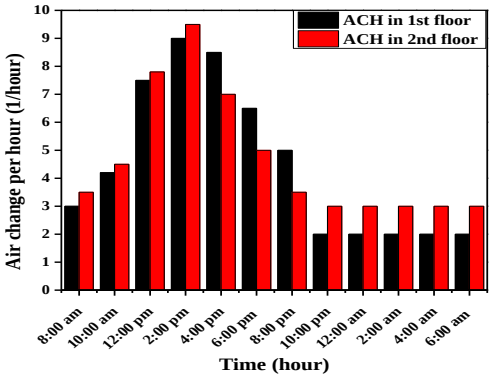

Figure 20 ACH values when using Block-shaped wax

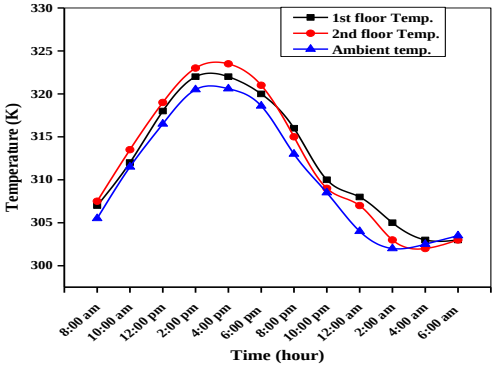

Figure 21 Temperature values when using Block-shaped wax

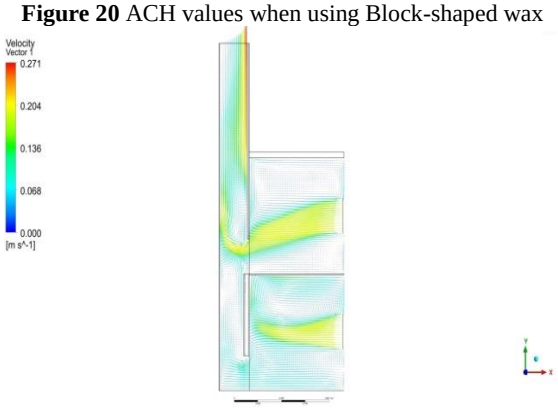

Figure 22 Velocity vector when using Block-shaped wax at 12 p.m.

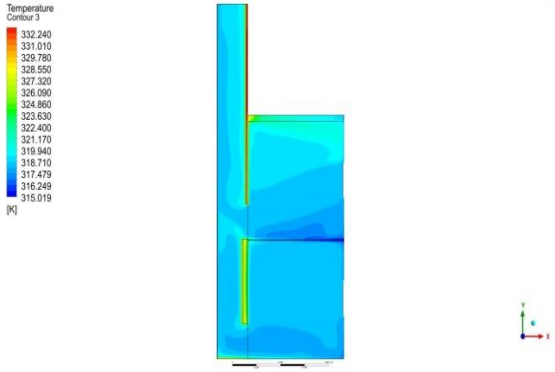

Figure 23 Temperature contour when using Block-shaped wax at 12 p.m.

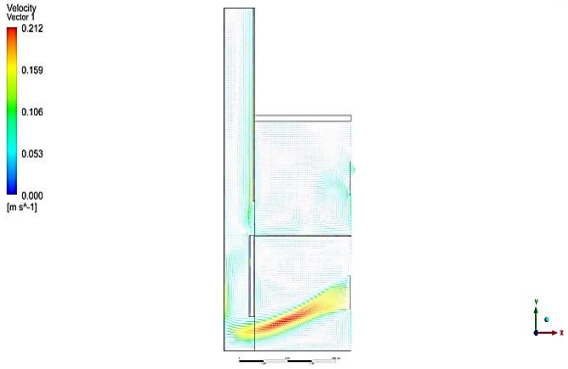

Figure 24 Velocity vector when using Block-shaped wax at 8 p.m.

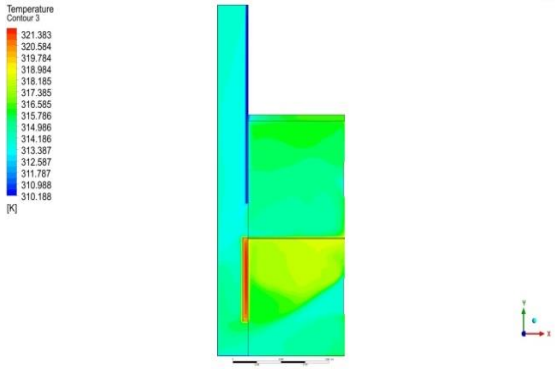

Figure 25 Temperature contour when using Block-shaped wax at 8 p.m.

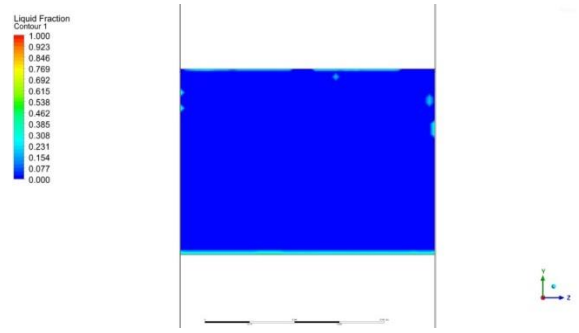

Figure 26 The liquid fraction contour of Block-shaped wax at 12 p.m.

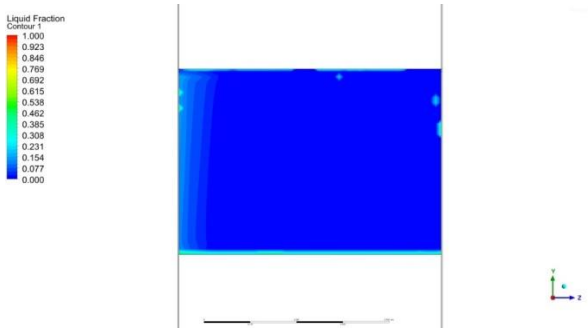

Figure 27 The liquid fraction contour of Block-shaped wax at 8 p.m.

5.2.3. RT- 42 paraffin wax

In the 3rd case , RT-42 wax was used as the ES, and the findings dealt with the ACH, internal temperatures of the two-story building throughout the day, and ventilation hours. The maximum ACH of the 1st floor was 10, which occurred at 2 p.m., while the minimum value was 2 at 2 to 6 a.m.. The highest and lowest amount of (ACH) were 9.5 and 3, respectively for the 2nd floor, as shown in figure 28. The average values were 5.75 and 5.375 on the 1st and 2nd floor, respectively.

Figure 29 displays the indoor temperatures of the two-story building. The results revealed that the greatest recorded temperature on the first floor was 323 k at 4 p.m., while the minimum temperature was 304 between 2 and 4 a.m. On the other side, the greatest and lowest temperatures recorded on the second floor were 323 k and 303 k, respectively. While the average indoor temperature were 312.625 k and 312.916 k, respectively.

Also, the ventilation process started at 8 a.m. and ended at 12 a.m. The velocity vectors, temperature, and liquid fraction contours plotted at 12 p.m. and 12 a.m. are shown in Figures 30 to 35, respectively. The shapes of the liquid fraction showed that this type of wax is the most easy to melt due to its low melting point, which is equal to 43 degrees Celsius. The simulation results showed that the amount of liquid wax was estimated at 0.7, 1, and 0.55 at 12 pm, 6 pm and 12 am, respectively.

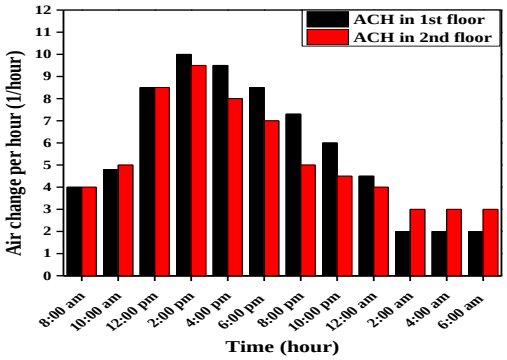

Figure 28 ACH when using RT-42 wax

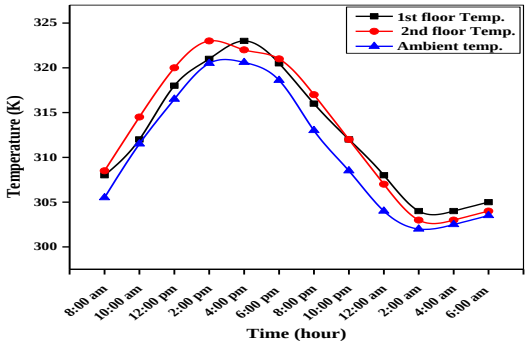

Figure 29 Ave. indoor temperature when using RT-42 wax

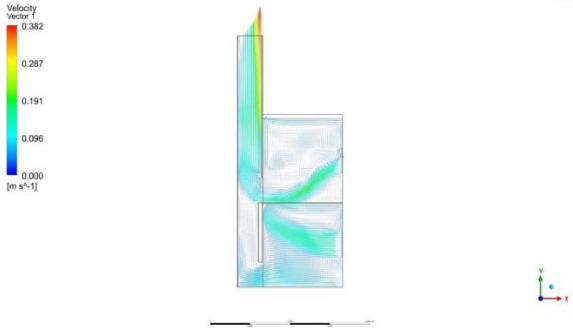

Figure 30 velocity vector when using RT-42 wax at 12 p.m.

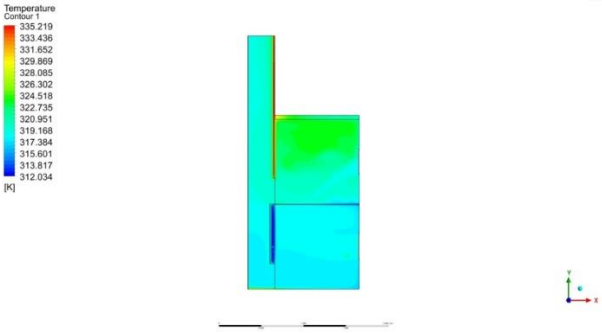

Figure 31 Temperature contour when using RT-42 wax at 12 p.m.

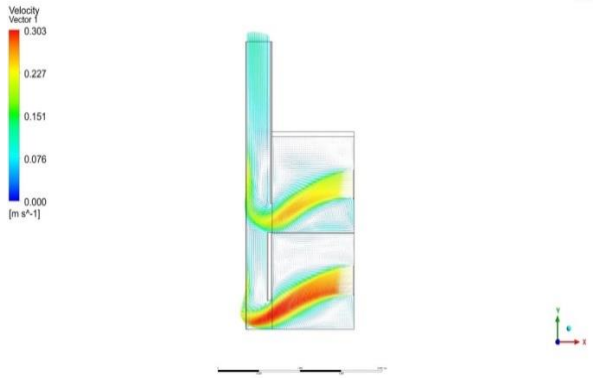

Figure 32 velocity vector when using RT-42 wax at 12 a.m.

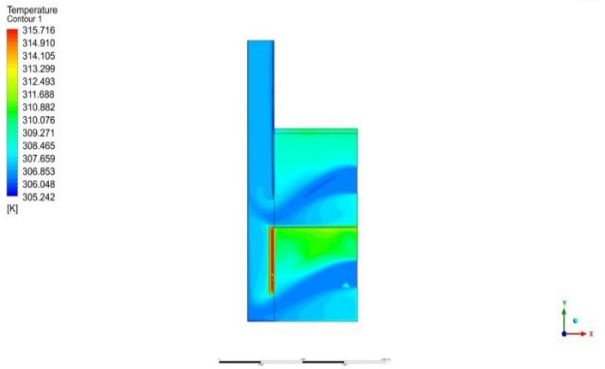

Figure 33 Temperature contour when using RT-42 wax at 12 a.m.

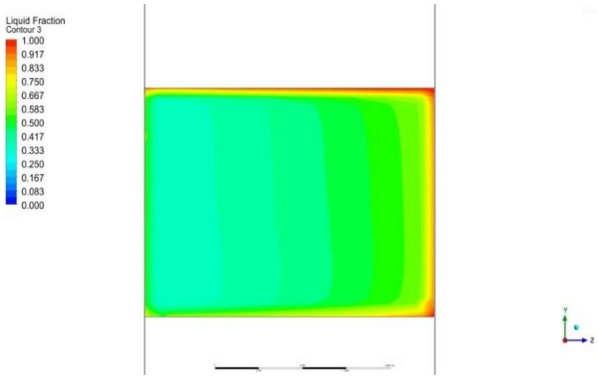

Figure 34 Liquid fraction contour of RT-42 wax at 12 p.m.

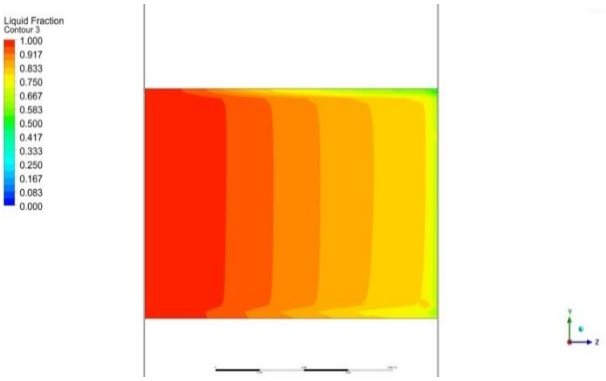

Figure 35 Liquid fraction contour of RT-42 wax at 12 a.m.

5.3 Comparison between ES types

The comparisons were done between the three varieties of wax and the first model based on three factors: average ACH, interior temperature, and ventilation duration so that to specify the best wax type.

Figures 36 and 37 show a comparison between the three types of wax and the 1st model in average ACH and average indoor temperature, respectively.

The results showed that the improvement percent in ACH for Al-dura and RT-42 wax were very similar about 18 % and 10 % for 1st and 2nd floor, respectively when comparing with the 1st model. While in cases of block wax the ACH reduced by 7.4 % in the 1st floor and 4.123 % in the 2nd floor.

Besides, the temperature reduced by 1.2 k and 0.86 k for 1st and 2nd floor in case of Al-dura wax when comparing with 1st model. While, the reduction in temperature in case of block and RT-42 were 0.71 k and 0.25 k, respectively in the 1st floor and for the 2nd floor, it was 0.42 k and 0.29 k, respectively.

Finally, the ventilation process took place for 5 hours after sunset in case of Al-dura and RT-42 paraffin wax, while in block-shaped wax it lasted to one hour after sunset.

The average ACH value in the instance of Al-dura and RT-42 wax was the highest in the prior results for two reasons. The 1st reason is the longest period of ventilation after sunset, while the 2nd reason is most of the wax material melted and reached the melting point at 2 p.m. As a result, the absorber wall is maintained at a high temperature (melting temperature of wax) for the rest of the daylight period while in the other cases the absorber wall cooled faster because of the high melting point of the other waxes. As a result of the wax's high melting temperature, thermal energy cannot be stored during the day due to the wax's inability to melt, which causes rapid heat loss.

Also, the reason behind the lowest temperature that registered in the case of Al-dura wax is because of the highest ACH which works on replacing the indoor hot air in the building with fresh outdoor air. It could be concluded from the foregoing that the best type of wax is Al-dura paraffin wax.

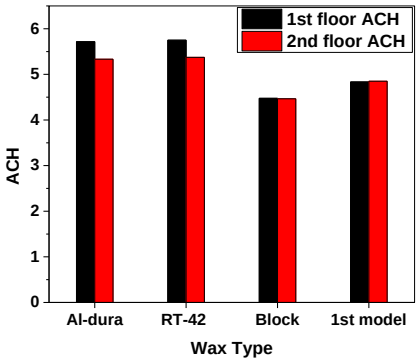

Figure 36 ACH comparison

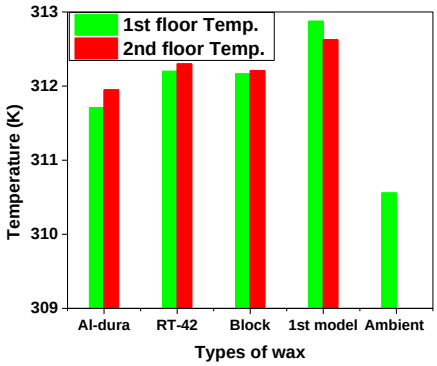

Figure 37 Temperature comparison

6. CONCLUSIONS

The solar chimney integrated with PCM is considered a good solution to extend the ventilation period after sunset. Numerical results showed that compared with 1st model, the ACH in the 2nd model increased by 18.34 % for 1st floor and 9.98 % for 2nd floor in the case of Al-dura wax. While in case of RT42, ACH increased by 18.97 % and 10.78 % on 1st and 2nd floors. But, in case of the block-shaped wax, the ACH was decreased by 7.4 % and 4.123 % on 1st and 2nd floors, respectively. On the 1st and 2nd floors, the temperature was decreased by 1.2 k and 0.68 k in case of Al-dura wax, whereas, in case of RT42 the reductions were 0.25 k and 0.29 k. while, in case of block-shaped wax, temperature decreased by 0.71 k and 0.42 k, when comparing with 1st model. As for the hours of ventilation after sunset, it was found that in both cases Al-dura and RT42 wax, the ventilation went on 5 hrs. after sunset. Whereas, in the case of block-shaped wax, the ventilation lasted for one hour. Finally, The melting point can be regarded as the most significant characteristic since, when taking into account the thermo-physical properties of the types of wax tested, it can be seen that the values are very close, with the exception of the melting point.

NOMENECLATURE

SC: Solar chimney
ES: Energy storage
PCM: Phase change material
CFD: computational fluid dynamics
V_{wind}: wind velocity
h_{conv}: convection heat transfer coefficient

FUNDING

The authors received no direct funding for this research.

AKNOWLDGEMENTS

The authors would like to express their gratitude to the staff of Al-dura Refinery for providing the research with the Al-dura paraffin wax. Thanks extended to the staff of labs. in the Iraqi Ministry of Science and Technology and the University of Technology/ Department of Materials for specifying the thermo physical properties of paraffin wax.

REFERENCES

1. Saleem, A. A., Bady, M., Ookawara, S., & Abdel-Rahman, A. K. (2016). Solar Chimney Design for Standard Ventilation Rate of Residential Buildings in a Hot-Arid Climate. *9Th International Conference on Indoor Air Quality, Ventilation & Energy Conservation in Buildings.*

2. Shi, L., Zhang, G., Yang, W., Huang, D., Cheng, X., & Setunge, S. (2018). Determining the

influencing factors on the performance of solar chimney in buildings. *Renewable and Sustainable Energy Reviews*, ***88***(September 2017), 223–238. https://doi.org/10.1016/j.rser.2018.02.033

3. Jubear, A. J., & Ghareer, A. D. (2018). Numerical investigations on solar chimney inclination angle for room ventilation. *International Journal of Engineering and Technology(UAE)*, ***7***(4), 1–9.
4. Hashim, H. S., Kassim, M. S., & Kadhim, H. H. (2020). Numerical investigation for natural ventilation enhancement in different models of solar chimney inside a room elicited from the concepts of the conventional chimney model. *Journal of Mechanical Engineering Research and Developments*, ***43***(5), 436–450.
5. Mohammed, H. J., Jubear, A. J., & Obaid, H. (2020). Natural ventilation in passive system of vertical two-stores solar chimney. *Journal of Advanced Research in Fluid Mechanics and Thermal Sciences*, ***69***(2), 130–146. https://doi.org/10.37934/ARFMTS.69.2.130146
6. Aboubakr, H., Taleb, T. A., & Janan, M. T. (2021). Simulation of Natural Ventilation on Building with Solar Chimney Under Climatic Conditions of Errachidia Morocco Zone. *Lecture Notes in Networks and Systems*, *211 LNNS*, 1191–1204. https://doi.org/10.1007/978-3-030-73882-2_109
7. Kaneko, Sagara, K., Yamanaka, T., & Kotani, H. (2006). Ventilation Performance of Solar Chimney mith Built-In Latent Heat Storage. *Proceedings of 10th International Conference on Thermal Energy Storage*, *September*.
8. Safari, M., & Torabi, F. (2014). Improvement of thermal performance of a solar chimney based on a passive solar heating system with phase-change materials. *Energy Equipment and Systems*, ***2***(2), 141–154. http://www.energyequipsys.com/article_9892_1015.html
9. Bin, L., Meixia, W., Qi, W., Shaoli, M., & Bennacer, R. (2017). Effect of the Position of the Phase Change Material (PCM Na2CO3•10H2O) on the Solar Chimney Effect. *Energy Procedia*, *139*, 462–467. https://doi.org/10.1016/j.egypro.2017.11.238
10. Salari, A., Ashouri, M., & Hakkaki-Fard, A. (2020). On the performance of inclined rooftop solar chimney integrated with photovoltaic module and phase change material: A numerical study. *Solar Energy*, ***211***(May), 1159–1169. https://doi.org/10.1016/j.solener.2020.10.064
11. Long, T., Li, W., Lv, Y., Li, Y., Liu, S., Lu, J., Huang, S., & Zhang, Y. (2022). Benefits of integrating phase-change material with solar chimney and earth-to-air heat exchanger system for passive ventilation and cooling in summer. *Journal of Energy Storage*, ***48***(January). https://doi.org/10.1016/j.est.2022.104037
12. A. D. Ghaeer and A. J. Jubear, "Numerical and experimental investigation of the ventilation performance of a building with multi-solar chimneys" Degree of Master of Science in Mechanical Engineering's Thesis, Wasit University, 2018.
13. Li, Y., & Liu, S. (2014). Experimental study on thermal performance of a solar chimney combined

with PCM. *Applied Energy*, *114*, 172–178. https://doi.org/10.1016/j.apenergy.2013.09.022

14. Fluent, A. (2013). MAN - ANSYS Fluent User' s Guide Releasde 15.0. *Knowledge Creation Diffusion Utilization*, *15317*(November), 724–746.
15. T. D. Canonsburg. (2013). ANSYS Fluent Theory Guide. *ANSYS Inc., USA*, *15317*(November), 814. http://www.afs.enea.it/project/neptunius/docs/fluent/html/th/main_pre.htm
16. McAdams, W.H., 1954. Heat Transmission, third ed. McGraw-Hill, Tokyo, Japan.
17. Abdeen, A., Serageldin, A. A., Ibrahim, M. G. E., El-Zafarany, A., Ookawara, S., & Murata, R. (2019). Solar chimney optimization for enhancing thermal comfort in Egypt: An experimental and numerical study. *Solar Energy*, *180*(October 2018), 524–536. https://doi.org/10.1016/j.solener.2019.01.063